LEAN METHANE-AIR FLAMES PROPAGATING UPWARD IN VERTICAL TUBES

V. Muntean and F. J. Higuera
E. T. S. Ingenieros Aeronáuticos, UPM, Madrid, Spain

Abstract
The upward propagation of a lean methane-air flame in a vertical tube is investigated. The shape and the velocity of the flame front are extracted from video records, and the velocity of the flow induced by the flame is measured with PIV using alumina particles to seed the gas. The thermophoretic drift of these particles relative to the gas is shown to cause an error in the PIV measurements in the transport region of the flame, where the temperature gradient is large. An iterative correction of the measured velocity is proposed that uses simplified, quasiunidimensional energy and species conservation equations to compute an approximation to the profile of gas temperature across the flame in terms of the profile of gas velocity. The correction is tested using synthetic velocity fields and applied along the axis of the tube. The results of the quasiunidimensional model also show that a conduction-radiation balance is approached in a region of low velocity that develops behind the flame front when the flammability limit is approached. Radiation losses from the combustion products in this region become then important and may cause the extinction of the flame.

Keywords: Lean premixed flames; upward propagation; thermophoresis

INTRODUCTION

In an attempt to normalize the determination of flammability limits, which in practical premixed systems depend on the conditions of the flow in addition to the kinetics of the combustion reactions, Coward and Jones (1952) carried out a comprehensive analysis of previous work and proposed a standard test to characterize reactive mixtures. A vertical tube of 51 mm ID and 1.8 m long, open at the bottom and closed at the top, is filled with the mixture to be tested, which is ignited near the lower end of the tube. The mixture is said to be flammable if a flame is generated and propagates to the upper end of the tube. Levy (1965) noted that the shape and velocity of near limit flames propagating in this standard flammability tube are dominated by buoyancy forces and are similar to the shape and velocity of a bubble rising in the tube, except for extreme values of the Lewis number of the reactant that is depleted by the flame. Extinction at the flammability limit begins at the tip of the flame front. The limit concentration of the deficitary reactant changes when the radius of the tube is changed, in a manner that depends on the Lewis number of this reactant and possibly on other factors (Coward and Jones 1952, Babkin et al. 1982). Lewis and von Elbe (1961) and Jarosinski et al. (1982) pointed to flame stretch as a cause of extinction at the flammability limit, and von Lavante and Strehlow (1983) approximately computed the flow of the fresh gas above the flame and found that the stretch is mainly due to the strain rate of the flow, which scales with the inverse of the square root of the tube radius, and that it is maximum at the tip of the flame front and of the right order to extinguish the flame (see Higuera 2011 for a more recent computation that includes the flow on both sides of the flame front). The issue of preferential diffusion in stretched flames was taken up by Shoshin et al. (2008). Since a positive stretch strengthens the flame when the Lewis number of the reactant that is depleted is below unity (Williams 1985), the limit concentration of such reactant should

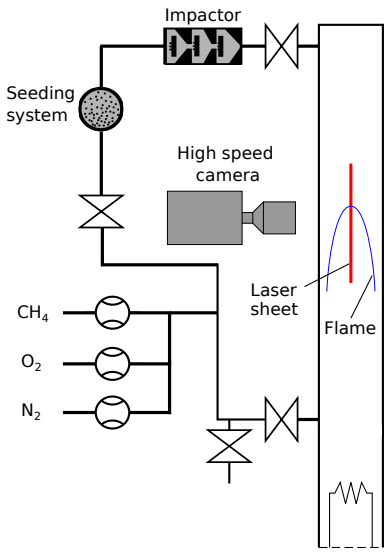

Figure 1: Sketch of the experiment

decrease with the radius of the tube. However, from their analysis, Shoshin et al. (2008) concluded that these effects cannot always explain the observed trends. Later, Shoshin and Jarosinski (2009) and Shoshin et al. (2010) proposed that heat losses from the flame due to the effect of radiation in a low velocity region that appears below very lean flames may explain the observed extinction.

Thermophoretic forces acting on small particles suspended in a gas whose temperature is not uniform cause these particles to drift away from hot regions of the gas with a velocity proportional to the local temperature gradient. When this velocity is not small compared to the velocity of the gas, the effect is detrimental to the accuracy of LDV and PIV measurements, which rely on the assumption that seeding particles follow the motion of the gas.The importance of thermophoresis in flame-related studies was demonstrated by Rosner et al. (1992) and Gomez and Rosner (1993). Discrepancies between measured and computed velocity profiles in strained flames were investigated, among others, by Chelliah et al. (1990) for diffusion flames and Sung et al. (1996) for premixed and diffusion flames.

In this paper, we report an experimental investigation of very lean methane-air flame fronts propagating upward in a tube. The shape and velocity of the flame front and the velocity of the gas around the flame are measured using photographic and PIV techniques. An approximate correction of the PIV results to account for the thermophoretic drift of the seeding particles is proposed that is based on simplified, quasiunidimensional model conservation equations for the energy and the reactants across the flame. The model determines an approximation to the temperature profile and the thermophoretic drift across the flame in terms of the gas velocity profile, which can thus be corrected in an iterative manner. The model is also used downstream of the flame, where it shows that radiation losses from the combustion products in a region of low velocity (relative to the flame) that appears behind very lean flames may account for the extinction of the flame at the flammability limit.

EXPERIMENTAL SETUP AND TECHNIQUES

The experimental apparatus has been described elsewhere (Muntean and Higuera 2015); only a brief summary is given here. A quartz tube of 54 mm internal diameter and 1.9 m

long is filled from the upper end with a mixture of 99.5%-pure methane and dried air or synthetic air made from ultrapure oxygen and nitrogen. The mixture, with a selected equivalence ratio, flows through the tube for at least 3 minutes in order to evacuate residual gases from previous runs. Mass flow controllers (EL-Bronkhorst calibrated with Ritter TG05 or TG10 drum-type gas meters) are used to separately measure the flow rate of each gas, achieving an accuracy of 1% in the equivalence ratio. The upper end of the tube is closed after it is filled with the fresh mixture, and the gas in the lower 15 cm of the tube is replaced with a slightly enriched mixture that enters through the lower valve in the sketch of Fig. 1. The purpose of this mixture is to facilitate launching the flame near the flammability limit; see Levy (1965), Shoshin et al. (2008) and Shoshin and Goey (2004). When the process is complete, the mixture is allowed to settle for about two minutes and is ignited with an electrical resistance located near the lower end of the tube, which remains open.

The shape and velocity of the flame front that rises in the tube are extracted from the video record of a camera that images a region of the tube about 15 cm long at 100 frames per second with a resolution of 15–20 pixel/mm. The Canny algorithm with a Laplacian of Gaussian filter is used to extract the contour of the flame from the recorded images.

A PIV system consisting of a continuous 808 nm laser (Amtron LS453) with a cylindrical sheet-forming lens and a high speed camera (NAC Memrecam HX-3) with a Nikkor Micro 60 mm objective is used to measure the velocity of the gas around the flame. The laser sheet is shone through the vertical axis of the tube, and the camera images a region of about 68 mm with a resolution of 32 pixel/mm. Alumina particles (Metalograph) are used to seed the gas. These particles are produced in the fluidized bed sketched in the upper part of Fig. 1 and enter the tube with the fresh mixture after going through an impactor that suppresses the largest particles. Particles with nominal diameters of 0.3 μm, 1 μm and 5 μm have been tried. The actual size distributions of the particles downstream of the impactor have been measured with DMA (TSI SMPS3938) and laser diffraction (Sympatec) size spectrometers, and from SEM micrographs. These measurements reveal fairly wide distributions of diameter, with a single maximum at a diameter somewhat smaller than the nominal value given by the supplier. The distributions extend into the tens of nanometers range, but these small particles are not expected to play a role in our PIV measurements, as they are well into the range of Rayleigh scattering where the intensity of scattered radiation decreases as the sixth power of the diameter scaled with the wavelength of the laser light. Globular agglomerates of tens of particles, with diameters of the order of the nominal value, also appear in the SEM images, as well as some larger aggregates which for the most part should be suppressed by the impactor. Particles of 0.3 μm nominal diameter were discarded as they are poor scatterers of the laser light used. Thermophoretic effects are important for all the particles used, which therefore fail to follow the gas in the transport region of the flame where the temperature gradient is large. An analysis of this effect and a possible correction of the PIV measurement are presented in the following section.

THERMOPHORESIS

Thermophoretic force and drift velocity

The thermophoretic force acting on a spherical particle of radius a immersed in a gas is of the form

$$\boldsymbol{F}_{TP} = -\mu a f_{TP} \nu \boldsymbol{\nabla} \ln T, \tag{1}$$

where $\nu = \mu/\rho$; ρ, T and μ are the density, temperature and viscosity of the gas; and $f_{TP}(\mathrm{Kn}, \Lambda)$ is a function of the Knudsen number, $\mathrm{Kn} = \ell/a$, where $\ell = 2\mu/\rho c$ with

$c = \sqrt{8R_g T/\pi}$ is the mean free path of the gas molecules, and of the gas-to-particle conductivity ratio Λ. Simple expressions for this function exist for small and large values of the Knudsen number, in the hydrodynamic and free molecular regimes, whereas correlations are available for $\mathrm{Kn} = O(1)$. A simple correlation proposed by Talbot et al. (1980) that spans the whole range of Knudsen numbers is

$$f_{TP} = \frac{12\pi C_s \left(\Lambda + C_t \,\mathrm{Kn}\right)}{\left(1 + 3C_m \,\mathrm{Kn}\right)\left(1 + 2\Lambda + 2C_t \,\mathrm{Kn}\right)}, \tag{2}$$

where $C_s = 1.17$, $C_t = 2.18$ and $C_m = 1.14$. Alternative, more accurate results have been proposed by Beresnev and Chernyak (1985), but the simple expression (2) will be assumed here.

The hydrodynamic force acting on the particle due to its relative motion to the gas is, for small values of the gas-to-particle density ratio and of the Reynolds number of the slip flow,

$$\boldsymbol{F}_v = -\frac{6\pi\mu a}{f_C(\mathrm{Kn})}\left(\boldsymbol{v}_p - \boldsymbol{v}\right) \quad \text{with} \quad f_C = 1 + \mathrm{Kn}\left[A + B\exp\left(-C/\mathrm{Kn}\right)\right], \tag{3}$$

where $\boldsymbol{v}_p$ and $\boldsymbol{v}$ are the velocities of the particle and the gas, and $f_C(\mathrm{Kn})$, with $A = 1.20$, $B = 0.41$ and $C = 0.88$, is the Cunningham correction factor to Stokes law for non-small values of the Knudsen number.

Using (1) and (3), the equations of motion of the particle become

$$m\frac{\mathrm{d}\boldsymbol{v}_p}{\mathrm{d}t} = \boldsymbol{F}_v + \boldsymbol{F}_{TP} + m\boldsymbol{g} \quad \text{and} \quad \frac{\mathrm{d}\boldsymbol{x}_p}{\mathrm{d}t} = \boldsymbol{v}_p \quad \text{with} \quad m = \frac{4}{3}\pi a^3 \rho_p, \tag{4}$$

where $\boldsymbol{x}_p$ is the position of the particle, $\boldsymbol{g}$ is the acceleration of gravity, and ρ_p is the density of the solid. When the effects of the inertia of the particle and the gravity can be neglected, the balance $\boldsymbol{F}_v + \boldsymbol{F}_{TP} = 0$ gives the thermophoretic drift velocity of the particle relative to the gas as

$$\boldsymbol{v}_{TP} \equiv \boldsymbol{v}_p - \boldsymbol{v} = -\nu\alpha_{TP}\boldsymbol{\nabla}\ln T \quad \text{with} \quad \alpha_{TP} = \frac{f_{TP} f_C}{6\pi}. \tag{5}$$

The coefficient α_{TP} tends to 0.55 in the free molecular limit $\mathrm{Kn} \to \infty$ and takes very small values in the hydrodynamic limit $\mathrm{Kn} \to 0$ when $\Lambda \ll 1$. This coefficient is shown in Fig. 2(a) as a function of the gas temperature for alumina particles of various radii (density 4000 kg/m^3, thermal conductivity 30 W/m K). Here the approximation $\mu/\mu_u = (T/T_u)^\kappa$, with $\kappa = 0.75$, $T_u = 300$ K and $\mu_u = 1.78 \times 10^{-5}$ kg/m s, has been used for the gas viscosity. The Knudsen number of a particle of 1 μm radius increases from 6.28×10^{-2} to 0.47 when the gas temperature increases from 300 K to 1500 K, and α_{TP} increases accordingly.

In the transport region of a flame, $\boldsymbol{\nabla}\ln T \sim 1/\delta$, where δ is the flame thickness, which satisfies $\delta \sim \nu/U_L$ in terms of the burning velocity U_L (Williams 1985). Thus $v_{TP} \sim \nu\alpha_{TP}/\delta \sim \alpha_{TP}U_L$; the velocity of the particles significantly departs from the velocity of the gas when $\alpha_{TP} = O(1)$, which happens for small particles at high gas temperatures.

Synthetic velocities

To assess the effect of thermophoresis in the conditions of our experiment, the trajectories of seeding particles have been computed by solving (4) with synthetic velocity and temperature fields generated by a model of the flow and the flame. The model assumes that

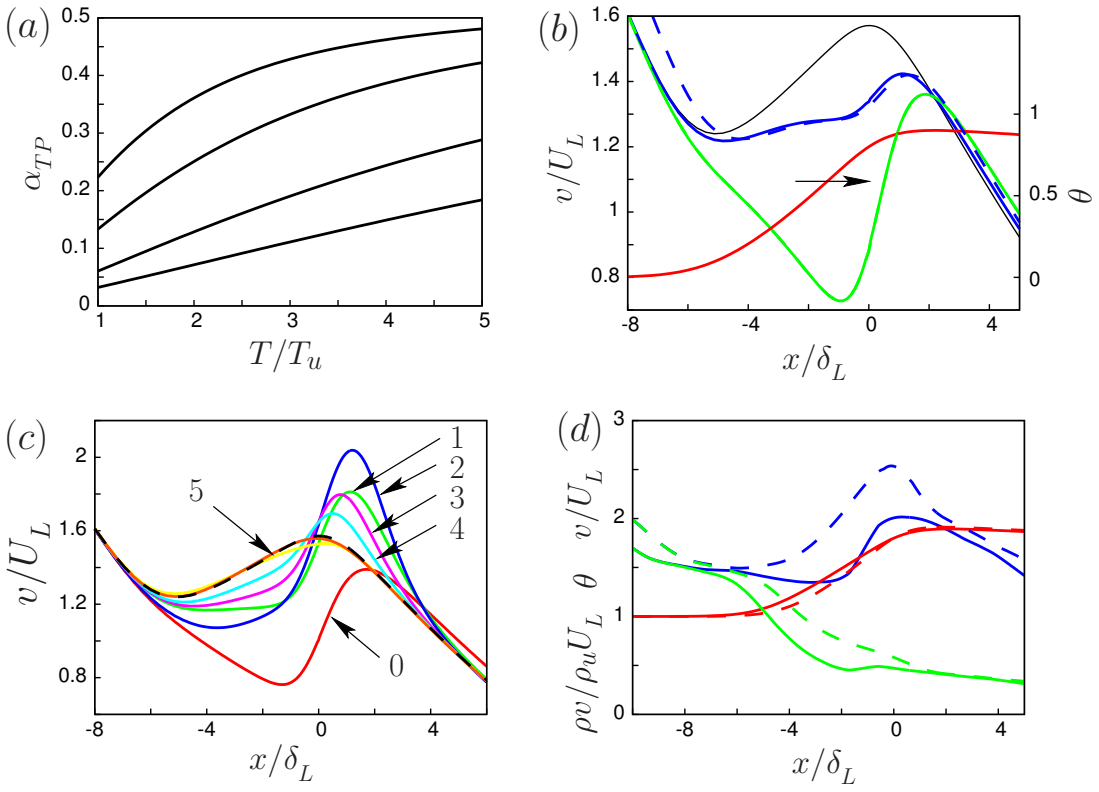

Figure 2: (a) Coefficient α_{TP} as a function of the gas temperature scaled with $T_u = 300$ K for $a = 1$, 2, 5 an 10 microns, increasing from top to bottom. (b) Profiles of gas velocity (black) and temperature (θ, red, right-hand side scale) along the axis of the tube, computed from (6)–(11) for $\phi = 0.546$, and profiles of particle velocity for $a = 1$ μm (green) and 5 μm (blue), computed from (4). The blue dashed curve is the velocity obtained from the balance $F_v + F_{TP} = 0$ for 5 μm particles. Velocities are scaled with the reference burning rate $U_L = 4.63$ cm/s, distance along the axis is scaled with the reference flame thickness $\delta_L = D_{Tu}/U_L = 0.43$ mm, and $\theta = (T - T_u)/(T_e - T_u)$, where T_e is the equilibrium temperature of the mixture computed with the Cantera software. (c) Corrected gas velocity for $\phi = 0.546$ from successive iterations for $a = 1$ μm seeding particles. The red curve, labeled 0, is the uncorrected (particle) velocity and the dashed curve is the true gas velocity. (d) Measured (blue, solid) and corrected (blue, dashed) velocity profiles for $\phi = 0.54$. Red and green curves are the temperature and mass flux profiles computed with the quasiunidimensional model for the measured (solid) and corrected (dashed) velocity profiles.

combustion occurs through a single irreversible Arrhenius reaction, uses Fick's diffusion law for all the species, and accounts for radiation losses from the CO_2 and H_2O generated by the flame by assuming that the gas is optically thin and using the statistical narrow band model to evaluate the Planck mean absorption coefficient (Fiveland 1984, Soufiani and Taine 1997). Assuming, in addition, that the flow is axisymmetric and stationary in a reference frame rising with the flame front, the governing equations take the form (see Higuera and Muntean 2014 for details)

$$\boldsymbol{\nabla}\cdot(\rho\boldsymbol{v})=0,\quad \rho\boldsymbol{v}\cdot\boldsymbol{\nabla}\boldsymbol{v}=-\boldsymbol{\nabla}p+\boldsymbol{\nabla}\cdot\tau'+\rho\boldsymbol{g},\quad \rho T=\rho_u T_u \tag{6}$$

$$\rho c_p\boldsymbol{v}\cdot\boldsymbol{\nabla}T=\boldsymbol{\nabla}\cdot(\rho c_p D_{_T}\boldsymbol{\nabla}T)+qw-L,\quad \rho\boldsymbol{v}\cdot\boldsymbol{\nabla}Y_i=\boldsymbol{\nabla}\cdot\left(\frac{\rho D_{_T}}{\mathrm{Le}_i}\boldsymbol{\nabla}Y_i\right)-s_i w, \tag{7}$$

for $i=\mathrm{CH_4}$, $\mathrm{O_2}$, $\mathrm{CO_2}$ and $\mathrm{H_2O}$, with the boundary conditions

$$x\to-\infty:\ \boldsymbol{v}=U_0\boldsymbol{i},\ T=T_u,\ Y_{_{CH_4}}=\frac{\phi}{17.39+\phi},\ Y_{_{O_2}}=\frac{4}{17.39+\phi},\ Y_{_{CO_2}}=Y_{_{H_2O}}=0 \tag{8}$$

$$x\to\infty:\ \frac{\partial\boldsymbol{v}}{\partial x}=0,\ \frac{\partial T}{\partial x}=\frac{\partial Y_i}{\partial x}=0 \tag{9}$$

$$r=R:\ \boldsymbol{v}=U_0\boldsymbol{i},\ T=T_u,\ \frac{\partial Y_i}{\partial r}=0, \tag{10}$$

and

$$\left.\begin{aligned} w&=\rho B\exp\left(-T_a/T\right)Y_{_{CH_4}}Y_{_{O_2}},\quad \frac{\mu}{\mu_u}=\frac{\rho D_{_T}}{\rho_u D_{_{T_u}}}=\left(\frac{T}{T_u}\right)^{\kappa}\\ L&=4\sigma K\left(T^4-T_u^4\right)\quad\text{with}\quad K=\rho R^0 T\left(K_{_{CO_2}}\frac{Y_{_{CO_2}}}{W_{_{CO_2}}}+K_{_{H_2O}}\frac{Y_{_{H_2O}}}{W_{_{H_2O}}}\right).\end{aligned}\right\} \tag{11}$$

Here ρ, T, p and $\boldsymbol{v}$ are the density, temperature, pressure and velocity of the gas; τ' is the viscous stress tensor given by the Navier-Poisson law; Y_i, W_i and Le_i are the mass fractions, molecular masses and Lewis numbers of the different species; μ and $D_{_T}$ are the gas viscosity and thermal diffusivity, which are taken to increase as powers of the temperature, and c_p is the specific heat, which is taken to be constant; x and r are downward distance along the axis of the tube and distance to the axis, respectively, and $\boldsymbol{i}$ is a unit vector pointing downwards; the subscript u denotes conditions of the fresh gas above the flame, and $\phi=4Y_{_{CH_4u}}/0.23\left(1-Y_{_{CH_4u}}\right)$ is the equivalence ratio; U_0 is the upward velocity of the flame front, which is an eigenvalue of the problem; R is the radius of the tube; q is the heat released per unit mass of methane burnt, and $s_{_{CH_4}}=1$, $s_{_{O_2}}=4$, $s_{_{CO_2}}=-11/4$ and $s_{_{H_2=}}=-9/4$; the frequency factor B and the activation temperature T_a are chosen for the single reaction model to reproduce the planar flame velocity computed with the GRI-Mech 3.1 scheme in the range of equivalence ratios of interest (Higuera and Muntean 2014); $K_{_{CO_2}}$ and $K_{_{H_2O}}$ are functions of the temperature computed and tabulated by Ju et al. (1999); and σ and R^0 are the Stefan-Boltzmann and universal gas constants. Values of the parameters involved are $D_{_{T_u}}=2\times10^{-5}$ m^2/s, $c_p=10^3$ J/kg K, $\mathrm{Le}_{_{CH_4}}=1$, $\mathrm{Le}_{_{O_2}}=1.05$, $\mathrm{Le}_{_{CO_2}}=1.39$, $\mathrm{Le}_{_{H_2O}}=0.83$, $q=5.01\times10^4$ kJ/kg, $T_a=18750$ K, B such that $U_{_L}=4.63$ cm/s for $Y_{_{CH_4u}}=0.03$ (Davis et al. 2002), and $R=27$ mm.

Figure 2(b) shows profiles of gas velocity (black) and temperature (red) along the axis of the tube in the region of the flame for a value of the equivalence ratio $\phi=0.546$. The velocity of the gas first decreases on approaching the flame front from above, then increases on crossing the flame front due to the gas thermal expansion, decreases again downstream of the flame due to the buoyancy force acting on the burnt gas, and finally

increases at some distance downstream of the flame front (not shown in the figure) due to the convergence of the burnt gas that crosses the flame at different points of the front. The velocity of a seeding particle along the axis is computed from (4) assuming that the initial particle velocity (relative to the flame) is equal to velocity U_0 of the gas. The result is also shown in Fig. 2(b) for particles of radii $a = 1$ μm (green curve) and 5 μm (blue curve). As can be seen, the smaller particles are significantly delayed by thermophoresis inside the flame, where the temperature rapidly increases in the streamwise direction and $F_{TP} < 0$, and they move slightly faster than the gas downstream of the flame, where the temperature slowly decreases in the streamwise direction due to radiation losses. The effects of the inertia and the gravity are negligible for these particles; the green curve is indistinguishable from the velocity obtained from the balance $F_v + F_{TP} = 0$. The larger particles are less affected by thermophoresis, but the effects of the inertia and the gravity are important for them. These particles always fall faster than the gas, and the velocity difference is largest upstream of the flame front, where the gas undergoes a continuous deceleration that the large particles fail to follow. The blue dashed curve shows the velocity obtained from the balance $F_v + F_{TP} = 0$.

Correction of thermophoretic drift

PIV results obtained with small seeding particles for which the effects of the inertia and the gravity are negligible could be corrected for thermophoretic drift if the temperature distribution of the gas were known. In the absence of this information, a simple procedure is proposed here that allows us to compute an approximation to the gas temperature using simplified forms of the energy and species conservation equations. These equations require the velocity of the gas as an input which should come from PIV measurements. Since the correct gas velocity is not known beforehand, an iteration is used to simultaneously refine the correction of the measured velocity and the approximate temperature distribution on which this correction is based. The simplified conservation equations can in principle be applied to any section of the flame front, using information on the local normal. However, they are used here only at the uppermost point of the front, where the normal and the velocity of the gas, $v(x)$ in what follows, are vertical.

The simplified equations are derived from equations (7) taking advantage of the small thickness of the flame compared to the curvature radius of the flame front (of the order of the radius of the tube) to neglect radial diffusion of species everywhere in the flow field and radial conduction of heat in the transport region of the flame, while the radial conduction term of the energy equation is approximated downstream of the flame by $\rho c_p D_T \beta \left(T_b - T\right)/R^2$, where T_b is the final combustion temperature, R is the radius of the tube, and $\beta = 15$ is a model parameter whose value is chosen for the temperature obtained from the simplified equations to match the solution of (6)–(11) in a number of cases (see Muntean and Higuera 2015). The simplified equations are

$$\begin{aligned} \rho c_p v \frac{\mathrm{d}T}{\mathrm{d}x} &= \frac{\mathrm{d}}{\mathrm{d}x}\left(\rho c_p D_T \frac{\mathrm{d}T}{\mathrm{d}x}\right) + \rho c_p D_T \beta \mathcal{H}(T) \frac{T_b - T}{R^2} + qw - L, \\ \rho v \frac{\mathrm{d}Y_i}{\mathrm{d}x} &= \frac{\mathrm{d}}{\mathrm{d}x}\left(\frac{D_T}{\mathrm{Le}_i}\frac{\mathrm{d}Y_i}{\mathrm{d}x}\right) - s_i w, \end{aligned} \tag{12}$$

where $\mathcal{H}(T)$ is an indicator function equal to zero upstream of the temperature maximum an equal to one downstream. These equations are to be solved with the boundary conditions (8) and (9) for the temperature and the species mass fractions, and with the reaction and radiation terms given by (11). For a given $v(x)$, the equivalence ratio ϕ is iteratively computed for the mass flux ρv to vary smoothly across the flame. The difference between

the value of the equivalence ratio thus determined and its actual experimental value is a measure of the accuracy of the model.

The iterative correction of the PIV measured velocity proceeds as follows. The measured velocity, $v_m(x)$ say, is first used for $v(x)$ in (12). The temperature profile computed from these equations is used to evaluate the thermophoretic drift velocity $v_{TP}(x)$ from (5) and compute a corrected gas velocity $v(x) = v_m(x) - v_{TP}(x)$. This is carried again to the simplified equations (12) and the computation is iterated until the corrected gas velocity converges.

As a test, the iterative procedure has been applied to the synthetic particle velocity determined from (4) with the gas velocity and temperature fields obtained from (6)–(11). Assuming $a = 1$ μm, the velocity of the particles is given by the green curve of Fig. 2(b), which plays the role of $v_m(x)$, while the true gas velocity is given by the black curve. Figure 2(c) shows the corrected gas velocities obtained in successive iterations. As can be seen, the corrected gas velocity is indistinguishable from the true velocity (dashed curve in Fig. 2(c)) after six iterations.

RESULTS AND DISCUSSION

Steadily rising flame fronts consisting of a rounded cap and a nearly cylindrical skirt are obtained after an initial transient when wall temperature perturbations and residual motions of the gas are minimized. As it has been often noted, the shape of the upper cap and the velocity of very lean flame fronts are similar to those of a bubble rising in the tube. The measured flame front velocity is $U_0 = 24$ cm/s and depends little on the equivalence ratio in a range of values of this variable around the flammability limit, which is about $\phi = 0.525$ in our experiment. For comparison, the velocity of a bubble rising in this tube is 22 cm/s according to Davies and Taylor (1950) formula for a heavy-to-light fluid density of 5, while the burning velocity U_L of a planar flame with the same equivalence ratio is much smaller, of only a few centimeters per second. This disparity of velocity scales allows to explain the observed shape and velocity of the flame front. Buoyancy force pushes the burnt gas upward so that, in a reference frame moving with the flame front, the incoming fresh gas is decelerated and moves radially outward on approaching the front, much as the flow above a bubble. Also as for a bubble, pressure variations in the burnt gas behind the flame are small compared to the dynamic pressure of the fresh gas, due to the small density of the burnt gas. Finally, due to the small burning velocity of the flame, its tip lies close to the stagnation point of the equivalent bubble flow, and the rest of the flame is close to a streamline through this point. The length of the skirt increases when the equivalence ratio, and thus the burning velocity of the flame, is decreased.

Figure 3 shows the velocity of the gas relative to the flame for $\phi = 0.53$ (near the flammability limit) and 0.54. These velocity fields are obtained by substracting the upward velocity of the flame front from the PIV measured velocity. The results are not corrected for thermophoresis, whose effect, however, is small outside of the flame. Comparison of the two fields shows that the flow above the flame front displays the features discussed above and is nearly independent of the equivalence ratio, while the flow below the flame front develops a region of low velocity (relative to the flame) as the flammability limit is approached. The size of this region scales with the radius of the tube, and in some cases, like the one shown in Fig. 3(a), includes recirculation of the burnt gas. The residence time of the gas in the region of low velocity can be very large. As will be seen below, this increases the importance of radiation losses (mainly from CO_2 and H_2O) to such an extent as to affect the flame and eventually cause its extinction, despite the small concentrations of the radiating species.

The measured velocity of the gas along the axis of the tube has been corrected for

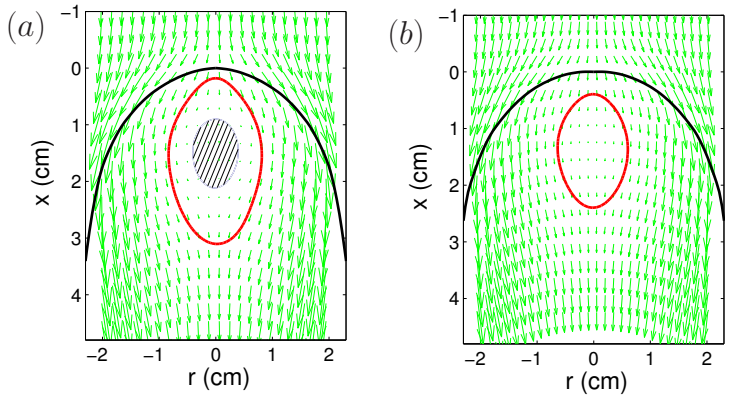

Figure 3: PIV velocity field of the gas relative to the flame for $\phi = 0.53$ (a) and 0.54 (b). The black curve is the contour of the luminous region of the flame extracted from the video records. The red contour encloses the region of low velocity where $|\boldsymbol{v}| < 6$ cm/s. The velocity is negative (upward) in the hatched region of figure (a).

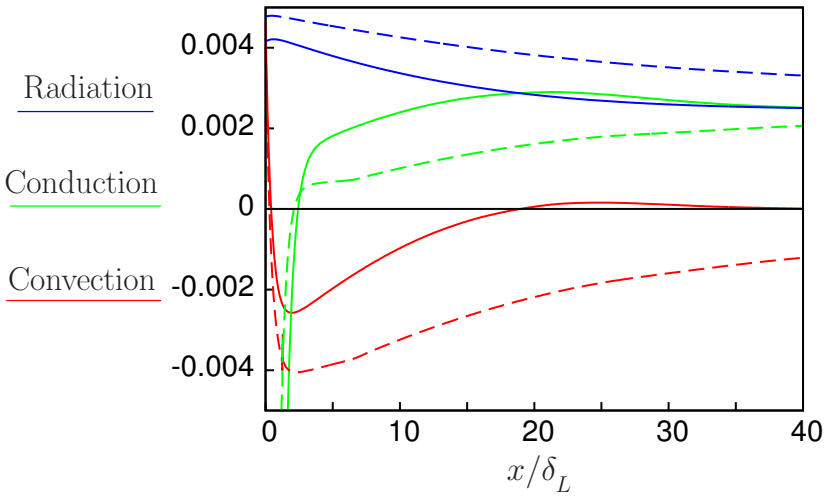

Figure 4: Convection (red), conduction (green) and radiation (blue) terms of the energy equation (12), all three scaled with $\rho_u U_L c_p (T_e - T_u)/\delta_L$, as functions of dimensionless distance from the point of maximum temperature, for $\phi = 0.53$ (solid curves) and 0.55 (dashed curves).

thermophoretic drift using the procedure described in the previous section. For this correction, the radius of the particles is taken to be $a = 1$ μm, as particles of this size are both abundant and more efficient laser light scatterers than smaller particles also present in the seeding. Figure 2(d) shows the effect of the correction for $\phi = 0.54$. The solid blue curve is the measured (uncorrected) velocity, and the dashed blue curve is the corrected velocity. The iteration scheme converged after four iterations. The solid and dashed red curves are the temperature profiles given by the quasiunidimensional model for the uncorrected and corrected gas velocity, respectively. The solid and dashed green curves are the corresponding mass fluxes, ρv. As can be seen, the magnitude of the velocity correction is significant within the flame, and the corrected mass flux is smoother than the uncorrected one. The values of the equivalence ratio yielded by the quasiunidimensional model are $\phi_{model} = 0.521$ and 0.539 for the uncorrected and corrected velocity profiles. The second one is nearer the real experimental value, suggesting that the correction has improved the velocity profile.

Computations with the quasiunidimensional model can be extended downstream of

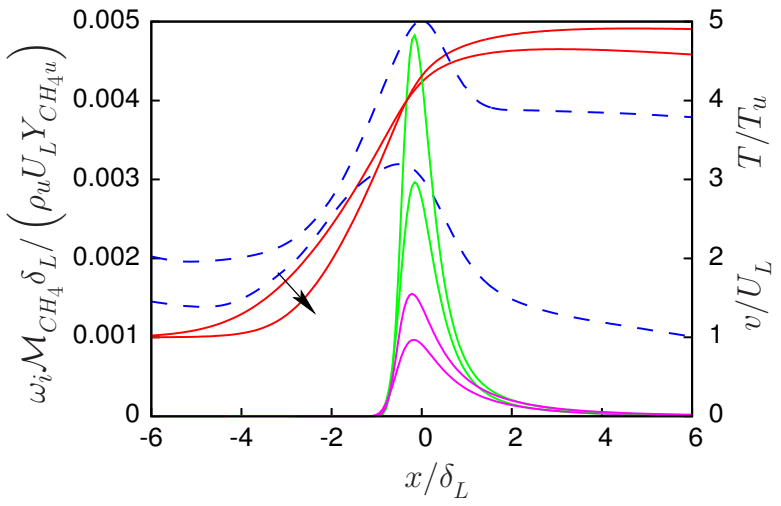

Figure 5: Profiles of temperature (red, right-hand scale) and rates of the radical production (green) and the radicals recombination (magenta) steps of the four step reduced scheme (left-hand scale) computed as functions of downward distance using the corrected velocity profiles (dashed blue, right-hand scale) for $\phi = 0.53$ and 0.55, increasing from bottom to top or as indicated by the arrow. The values of the equivalence ratio determined from the quasiunidirectional model are $\phi_{model} = 0.52$ and 0.53, respectively. Temperatures are scaled with $T_u = 300$ K, velocities with the reference burning rate $U_{_L} = 4.63$ cm/s, distances with the reference flame thickness $\delta_{_L} = D_{_{Tu}}/U_{_L} = 0.43$ mm, with $D_{_{Tu}} = 0.2$ cm^2/s, and reaction rates with $\rho_u \left(Y_{_{CH_4 u}}/W_{_{CH_4}}\right) U_{_L}/\delta_{_L}$.

the flame. Figure 4 shows the convection, conduction and radiation terms of the energy equation (12) evaluated in this region for $\phi = 0.53$ (solid curves) and 0.55 (dashed curves). At the lower value of the equivalence ratio, the small velocity of the gas downstream of the flame front renders convection negligible and reduces the energy equation to the conduction-radiation balance $\boldsymbol{\nabla} \cdot \boldsymbol{q} + L \approx 0$, with $\boldsymbol{q} = -\rho c_p D_{_T} \boldsymbol{\nabla} T$, in a large region of the flow field. This balance is quite different from the convection-radiation balance characteristic of a planar flame with heat losses (Williams 1985), a balance that is already approached by the results for the higher equivalence ratio in Fig. 4. The order of the heat flux in the conduction-radiation region is $q_b \sim L_b R$, where L_b is the radiation loss term in (11) evaluated in the burnt gas. The decrease of the final combustion temperature obtained by using this estimation in an enthalpy balance across the flame is $\delta T = O\left(L_b R/\rho_u c_p U_{_L}\right)$, where $U_{_L}$ is the flame burning velocity (see Muntean and Higuera 2015). This temperature decrease may easily be of the order of the Frank-Kamenetskii temperature T_b^2/T_a and may account for the extinction of the flame at the flammability limit.

The quasiunidimensional model of the previous section has been extended to replace the single step Arrhenius reaction by a more realistic four step reduced kinetic mechanism; see Sánchez et al. (2000) and references therein. Figure 5 shows the distributions of temperature and the rates of the radicals production and recombination steps computed using corrected gas velocity profiles for $\phi = 0.53$ and 0.55. The rate of the production step (green curves) decreases with the equivalence ratio faster than the rate of the recombination step (magenta curves), but it is not clear from these results that shortage of radicals to attack the fuel be the cause of extinction at the experimental flammability limit in our experiment.

CONCLUSIONS

The upward propagation of a lean methane-air flame front in a vertical tube has been investigated. Photographic records and PIV have been used to measure the shape and velocity of the flame front and the velocity of the gas around the front.

The effect of thermophoresis has been shown to be important for the particles used in PIV. These particles lag behind the gas in the transport region of the flame where the temperature gradient is large, and thus cause an error in the measured velocity. A correction of the PIV measurements has been proposed based on using simplified, quasi-unidimensional energy and species conservation equations to compute an approximation to the gas temperature and the thermophoretic drift, and on using this information to iteratively correct the velocity.

Results of the quasiunidimensional model show a conduction-radiation balance in a region of low velocity that develops behind the flame front then the flammability limit is approached. These results support the view that radiation losses from the combustion products in the low velocity region may cause the extinction of the flame at the flammability limit.

Acknowledgments. We are indebted to P. L. García-Ybarra (UNED) for useful discussions on thermophoresis and to G. García-Soriano (UNED) for his help in characterizing the size distributions of seeding particles. This work was supported by the Spanish MINECO through projects CSD2010-00010 and DPI2013-47372-C02-02.

*

References

Babkin, V. S., Zamashchikov, V. V., Badalyan, A. M., Krivulin, V. N. Kudryavtsev, E. A. and Baraton, A. N. 1982. Effect of tube diameter on homogeneous gas flame propagation limits, *Combust. Explos. Shock Waves* 18, 164–171.

Beresnev, S. and Chernyak, V. 1985. Thermophoresis on a spherical particle in a rarefied gas: Numerical analysis based on the model kinetic equation. *Phys. Fluids* 7, 1743–1756.

Chelliah, H. K., Law, C. K., Ueda, T., Smooke, M. D. and Williams, F. A. 1990. An experimental and theoretical investigation of the dilution, pressure and flow-field effects on the extinction condition of methane-air-nitrogen diffusion flames. *Proc. Combust. Inst.*, 503–511.

Coward, H. F. and Jones, G. W. 1952. *Limits of flammability of gases and vapors,* U. S. Bureau of Mines Bull. #503.

Davies, R. M. and Taylor, G. I. 1950. The mechanics of large bubbles rising through extended liquids and through liquids in tubes, *Proc. R. Soc. London A* 200, 375–390.

Davis, S. G., Quinard, J. and Searby, G. 2002. Markstein numbers in counterflow, methane- and propane-air flames: a computational study, *Combust. Flame* 130, 123–136.

Fiveland, W. A. 1984. Discrete-ordinates solutions of the radiative transport equation for rectangular enclosures, *ASME J. Heat Transfer* 106, 699–706.

Gomez, A. and Rosner, D. E. 1993. Thermophoretic effects on particles in counterflow laminar diffusion flames. Fiveland, W. A. 1984. *Combust. Sci. Technol.* 89, 335–362.

Higuera, F. J. 2011. Numerical simulation of the upward propagation of a flame in a vertical tube filled with a very lean mixture, *Combust. Flame* 158, 885–892.

Higuera, F. J. and Muntean, V. 2014. Effect of radiation losses on very lean methane/air flames propagating upward in a vertical tube, *Combust. Flame* 161, 2340–2347.

Jarosinski, J., Strehlow, R. A. and Azarbarzin, A. 1982. The mechanisms of lean limit extinguishment of an upward and downward propagating flame in a standard flammability tube. *Proc. Combust. Inst.* 19, 1549–1557.

Ju, Y., Guo, H., Liu, F. and Maruta, K. 1999. Effects of the Lewis number and radiation heat loss on the bifurcation and extinction of CH_4/O_2–N_2–He flames, *J. Fluid Mech.* 379, 165–190.

von Lavante, E. and Strehlow, R. A. 1983. The mechanism of lean limit flame extinction, *Combust. Flame* 49, 123–140.

Levy, A. 1965. An optical study of flammability limits, *Proc. R. Soc. London A* 283, 134–145..

Lewis, B. and von Elbe, G. 1961. *Combustion, Flames and Explosions of Gases,* Academic Press, New York, Chap. 5.

Muntean, V. and Higuera, F. J. 2015. Upward propagation of very lean methane-air flames in vertical tubes. *Flow, Turbulence Combust.* DOI 10.1007/s10494-015-9661-x.

Rosner, D. E., Mackowski, D. W., Tassopoulos, M., Castillo, J. and García-Ybarra, P. 1992. Effects of heat transfer on the dynamics and transport of small particles suspended in gases. *I & EC Res. (ACS)* 31, 760–769.

Sánchez, A. L., Lépinette, A., Bollig, M., Liñán, A. and Lázaro, B. 2000. The reduced kinetic description of lean premixed flames. *Combust. Flame* 123, 436–464.

Shoshin, Y. L. and de Goey, L. P. H. 2004. Experimental study of lean flammability limits of methane/hydrogen/air mixtures in tubes of different diameters, *Exp. Thermal Fluid Sci.* 34, 373–380.

Shoshin, Y. L., Gorecki, G., Jarosinski, J. and Fodemski, T. 2010. Experimental study of limit lean methane/air flame in a standard flammability tube using particle image velocimetry method, *Combust. Flame* 157, 884–892.

Shoshin, Y. L. and Jarosinski, J. 2009. On extinction mechanism of lean limit methane-air flame in a standard flammability tube. *Proc. Combust. Inst.* 32, 1043–1050.

Shoshin, Y. L., Tecce, L. and Jarosinski, J. 2008. Experimental and computational study of lean limit methane-air flame propagating upward in a 24 mm diameter tube, *Combust. Sci. Technol.* 180, 1812–1828.

Soufiani, A. and Taine, J. 1997. High temperature gas radiative property parameters of statistical narrow-band model for H_2O, CO_2 and CO, and correlated K-model for H_2O and CO_2. *Int. J. Heat Mass Transfer* 40, 987–991.

Sung, C. J., Kistler, J. S., Nishioka, M. and Law, C. K. 1996. Further studies on effects of thermophoresis on seeding particles in LDV measurements in strained flames. *Combust. Flame* 105, 189–201.

Talbot, L., Chen, R. K., Schefer, R. W. and Willis, D. R. 1980. Thermophoresis on particles in a heated boundary layer. *J. Fluid Mech.* 101, 737–758.

Williams, F. A. 1985. *Combustion Theory*, 2nd ed. Benjamin Cummings, Menlo Park, CA.